Journal of Materials Chemistry A

RSC Publishing

PAPER

View Article Online
View Journal | View Issue

Phosphorous–vacancy–oxygen defects in silicon

H. Wang,[a] A. Chroneos,*[bc] D. Hall,[d] E. N. Sgourou[e] and U. Schwingenschlögl*[a]

Cite this: *J. Mater. Chem. A*, 2013, **1**, 11384

Received 4th June 2013
Accepted 29th July 2013

DOI: 10.1039/c3ta12167d

www.rsc.org/MaterialsA

Electronic structure calculations employing the hybrid functional approach are used to gain fundamental insight in the interaction of phosphorous with oxygen interstitials and vacancies in silicon. It recently has been proposed, based on a binding energy analysis, that phosphorous–vacancy–oxygen defects may form. In the present study we investigate the stability of this defect as a function of the Fermi energy for the possible charge states. Spin polarization is found to be essential for the charge neutral defect.

I Introduction

Silicon (Si) is a mainstream material used in many microelectronic, photovoltaic, and sensor devices. Even though there have been intensive studies of the defect processes in Si for more than five decades, there are still defect–dopant associations that are not well understood.[1–5] Those can be essential considering that the dimensions of devices can be only a few nanometers with atomic effects becoming more and more important. Oxygen (O) and phosphorous (P) are key defects in Si. Their tendency to associate with lattice vacancies (V) leads to the well known A-centers ($V + O_i \rightarrow VO_i$, where O_i denotes interstitial O) and E-centers ($P + V \rightarrow PV$) which influence the properties of Si.[6]

The formation of A-centers and E-centers is of particular importance for Si-based imaging and spectroscopy sensors used in space, most specifically in charge-coupled device and complementary metal–oxide–semiconductor sensors. As the scientific goals of space missions, such as the visible light instruments on the future Euclid[7] and Gaia[8] missions, increase in complexity, the requirements on the precision of the sensors on board become increasingly demanding and the interaction with the radiation environment therefore increasingly important. High energy protons of the space radiation cause lattice displacement damage, giving rise to a supersaturation of Vs. When these Vs diffuse through the lattice and encounter P or O_i atoms they form stable E-centers and A-centers, respectively. The presence of such centers, known as traps, can impact the device performance and cause a smearing of the images produced. An understanding of the properties is necessary to improve devices through design as well as for the application of appropriate image correction algorithms, such as those employed on the Hubble space telescope and those due to be used for Gaia.[9,10]

Interestingly, in a recent study based on density functional theory it has been proposed that it is energetically favorable to form phosphorous–vacancy–oxygen (PVO_i) defects in Si.[11] In the following we therefore investigate the binding, ionization, and formation energies of the PVO_i defect with respect to the Fermi energy for the possible charge states.

II Methodology

The Vienna *ab initio* simulation package[12] is used, where the pseudopotentials are generated by the projector augmented wave method.[13] The defect structure is constructed based on a $2 \times 2 \times 2$ supercell that contains 64 Si atoms. A $3 \times 3 \times 3$ Monkhorst–Pack[14] type k-mesh is used and the cutoff energy for the plane waves is set to 400 eV. The supercell size, k-mesh, and cutoff energy have been checked to yield accurate results. The lattice constant of pure Si is optimized by the PBEsol[15] functional. This procedure is as accurate as calculations using the hybrid Heyd, Scuseria, and Ernzerhof (HSE) functional.[16,17] For each defect and charge state, the lattice parameters are kept constant (that of pure Si) and the atomic positions are relaxed for the forces on all atoms to decline below 0.01 eV Å^{-1}. Then the optimized structures are used for the HSE calculations with the screening parameter $\mu = 2.06$ Å^{-1}. The local part of the HSE functional is evaluated using the Perdew–Burke–Ernzerhof functional.[18] Finally, we apply the correction approach developed by Freysoldt *et al.*[19,20] on our finite size supercell calculations to eliminate interaction between the charged defects, *i.e.*, to treat them as isolated. The dielectric constant of Si entering the correction approach is taken from ref. 21.

The formation energies of the neutral and charged PV and PVO_i defects can be calculated using the relation[22]

$$\Delta E_{D,q}(\mu_e,\ \mu_a) = E_{D,q} - E_H + \sum_a n_a \mu_a + q\mu_e \qquad (1)$$

[a]*PSE Division, KAUST, Thuwal 23955-6900, Kingdom of Saudi Arabia. E-mail: Udo.Schwingenschlogl@kaust.edu.sa*

[b]*Engineering and Innovation, The Open University, Milton Keynes MK7 6AA, UK. E-mail: Alex.Chroneos@open.ac.uk*

[c]*Department of Materials, Imperial College, London SW7 2AZ, UK*

[d]*Department of Physical Sciences, The Open University, Milton Keynes MK7 6AA, UK*

[e]*University of Athens, Solid State Physics Section, Panepistimiopolis, Zografos 157 84, Athens, Greece*

where $E_{D,q}$ is the total energy of the defective cell with charge q and E_H is the total energy of the perfect cell. Moreover, n_a represents the numbers of atoms added to or removed from the defective cell and μ_a corresponds to their chemical potentials. Finally, μ_e is the Fermi energy, which is measured from the top of the valence band maximum (VBM) and has values in the band gap: $E_{VBM} \leq \mu_e \leq E_{VBM} + E_g$. The O chemical potential is calculated using α-quartz SiO_2 as $(E(SiO_2) - 3\mu_{Si})/6$.

To investigate the energetics of point defect association and cluster formation it is useful to calculate the binding energies of the clusters. For example, the binding energy of a substitutional P atom, an O_i atom, and a V to form a PVO$_i$ cluster in Si is given by

$$E_b(PVO_iSi_{N-2}) = E(PVO_iSi_{N-2}) - E(PSi_{N-1}) - E(O_iSi_N) - E(VSi_{N-1}) + 2E(Si_N) \quad (2)$$

where $E(PVO_iSi_{N-2})$ is the energy of a N atom supercell (here $N = 64$) containing $N - 2$ Si atoms, one P atom, one O_i atom, and one V. Furthermore, $E(PSi_{N-1})$ is the energy of a supercell with one P atom and $N - 1$ Si atoms, $E(O_iSi_N)$ is the energy of a supercell with one O_i atom and N Si atoms, $E(VSi_{N-1})$ is the energy of a supercell with one V and $N - 1$ Si atoms, and $E(Si_N)$ is the energy of a supercell with N Si atoms. Therefore, a negative binding energy corresponds to a defect cluster that is stable with respect to its point defect components.

III Results and discussion

In previous *ab initio* calculations[11] it was found that the energetically favorable PVO$_i$ defect in Si has the V in the middle between the P substitutional atom and the O_i (refer also to Fig. 1(g) of ref. 11). In that work next nearest neighbor arrangements were also studied but were deemed to be less favorable. The PVO$_i$ defect can be formed when an A-center encounters a P substitutional atom ($VO_i + P \rightarrow PVO_i$) or when a P$V$ pair encounters an O_i atom ($PV + O_i \rightarrow PVO_i$). It is important to identify the dominant charge states of the PVO$_i$ defect for different doping conditions. For the PBEsol functional, the total energy of the PV charge neutral state is lowered by less than 0.001 eV under spin polarization as compared to the spin degenerate case. However, spin polarization is more important for the PVO$_i$ charge neutral state due to a total energy decrease of 0.04 eV. Other charge states of the PV and the PVO$_i$ defects are found to be not sensitive to spin polarization. Hence, a spin polarized HSE calculation is only employed for the PVO$_i^0$ defect. Fig. 1 presents the formation energies of the PV and the PVO$_i$ defects, with respect to the Fermi energy, for various charge states. From Fig. 1(b) it is deduced that the PVO$_i^{+1}$ defect dominates up to a Fermi energy of 0.17 eV, above which the PVO$_i^0$ defect dominates up to 0.69 eV, above which the PVO$_i^{-1}$ defect dominates. Finally, above a Fermi energy of 1.02 eV the PVO$_i^{-2}$ defect is most stable, but only by a small amount of energy. Note that the formation energy of the PVO$_i^0$ defect is obtained by a spin polarized calculation.

We subsequently consider the PV defect for comparison with the PVO$_i$ defect. The PV^{+1} defect dominates up to a Fermi energy of 0.16 eV. Then the PV^0 defect is prevalent but only for a small range up to 0.17 eV, followed by the negatively charged states PV^{-1} (up to 0.24 eV) and PV^{-2}. For a Fermi energy in the range from 0.15 eV to 0.17 eV the formation energies of the PV^{-2}, PV^{-1}, PV^0, and PV^{+1} defects are close. The ionization energies of the PV and PVO$_i$ defects are summarized in Table 1.

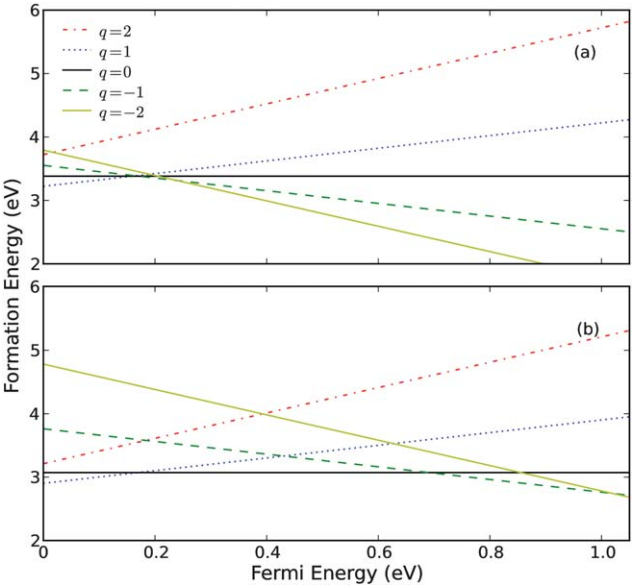

Fig. 1 Formation energies of the (a) PV and (b) PVO$_i$ defects, with respect to the Fermi energy.

Table 1 Ionization energies (in eV) for the PV and PVO$_i$ defects

Ionization energy	PV	PVO$_i$
(++/0)	—	—
(+/0)	0.16	0.17
(0/−)	0.17	0.69
(0/−−)	0.21	0.85
(−/−−)	0.24	1.02
(+/−)	0.17	0.43
(+/−−)	0.19	0.63
(++/−)	—	0.18
(++/−−)	0.02	0.39

The binding energies (refer to eqn (2)) of the PVO$_i^{-1}$, PVO$_i^0$, and PVO$_i^{+1}$ defects are −2.82 eV, −3.80 eV, and −2.86 eV, respectively. The equivalent binding energies of the PV^{-1}, PV^0, and PV^{+1} defects are −1.05 eV, −1.57 eV, and −0.74 eV, respectively. These differences of the binding energies are due to the formation of the O interstitial. Note that the latter is assumed to be charge neutral. Furthermore, the difference $E(PVO_i) - E(PV)$ deviates from the O chemical potential calculated using α-quartz SiO_2 by −0.31 eV, which suggests that the interaction between PV and O_i is stronger than that between O and Si in α-quartz SiO_2.

In Fig. 2 the shaded and unshaded densities of states (DOSs) indicate that the band gap of pure Si obtained by the HSE calculation is about 1.05 eV, which is in good agreement with

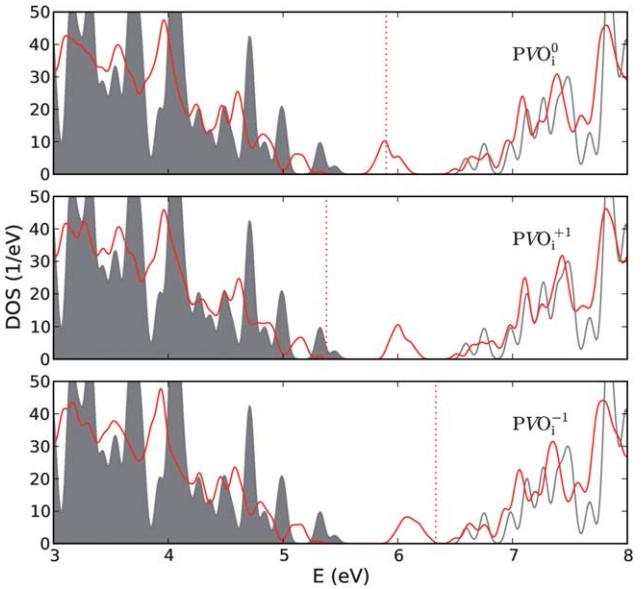

Fig. 2 Total DOSs of pure Si (gray) and Si with PVO_i cluster (red). The occupied states of pure Si are shaded. The Fermi energy of the PVO_i cluster is shown by a dotted line.

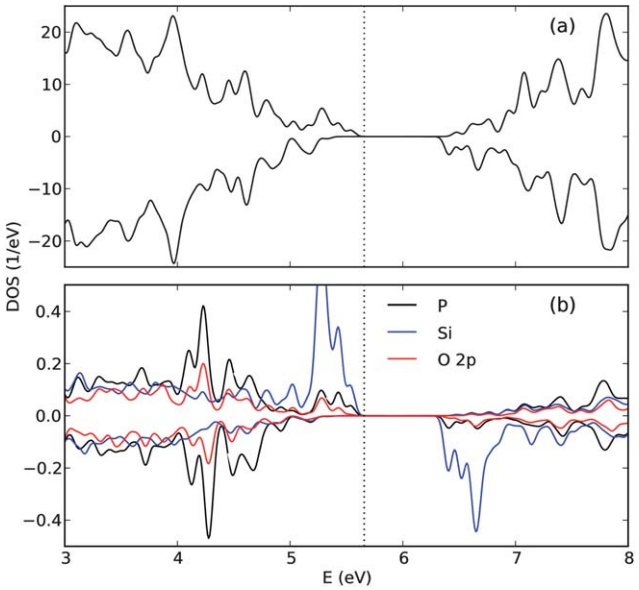

Fig. 3 Spin polarized (a) total DOS and (b) partial P 2s + 2p, Si 2s + 2p, and O 2p DOSs of Si with PVO_i cluster.

the experimental value of 1.17.[23] The spin degenerate DOS shows that the defect state of the PVO_i^0 cluster is half occupied, see the middle of the band gap, which causes the valence band to be located at a lower energy than in pure Si. However, the conduction band is rather close to that of pure Si. The defect state is contributed by all the atoms around the PVO_i^0 cluster. It is empty for PVO_i^{+1} and fully occupied for PVO_i^{-1}. The energetical positions of the valence and conduction bands remain similar for the different charge states of the PVO_i cluster, but the defect state shifts considerably. This is obvious for PVO_i^{-1}, where the energy gap between the defect state and the conduction band becomes small and the lower energy gap is enlarged. Fig. 1 illustrates that PVO_i^{+1} and PVO_i^{-1} dominate at low and high electron chemical potentials, respectively, which demonstrates that the unoccupied defect state (PVO_i^{+1}) and the fully occupied defect state (PVO_i^{-1}) are rather stable.

The peak at the Fermi level of PVO_i^0, as shown in Fig. 2, indicates that the spin degenerate scenario is unstable. Therefore, the spin polarized DOS of PVO_i^0 is presented in Fig. 3(a). The defect states split such that the total energy is lowered by 0.28 eV. We observe that the occupied half of the defect state merges to the valence band and the other half to the conduction band. Thus, the band gap changes to be 0.67 eV. The Si atom next to the *V* (having a dangling bond) shows a significant magnetic moment of 0.24 μ_B, while the moments of all other atoms are negligible. Only if spin polarization is taken into account the PVO_i^0 defect is low enough in energy to be favorable against the +1 and −1 charge states in a certain Fermi energy range (0.17 eV to 0.69 eV). Fig. 3(b) shows the DOSs of the P atom, of the Si atoms with significant magnetic moment, and of O for the PVO_i^0 cluster. The P and Si DOSs are presented as sums of the 2s and 2p states due to a strong s–p hybridization. The defect state is located between 5.1 eV and 5.7 eV, where P and O have minor contributions, while Si dominates. This fact indicates that the single dangling electron is well localized on the Si site and does not interact with P and O. For this reason, this Si atom has a relevant magnetic moment. When O is introduced into the P*V* defect, the dangling bonds of two Si atoms next to the *V* are eliminated. The DOS demonstrates a strong P–O hybridization. In this situation, the dangling electron of the third Si atom adjacent to the *V* interacts little with other atoms.

To explain why spin polarization is less important for the P*V* than for the PVO_i defect, we plot for the PV^0 cluster the total DOS and the partial DOSs of the P atom and of the three Si atoms

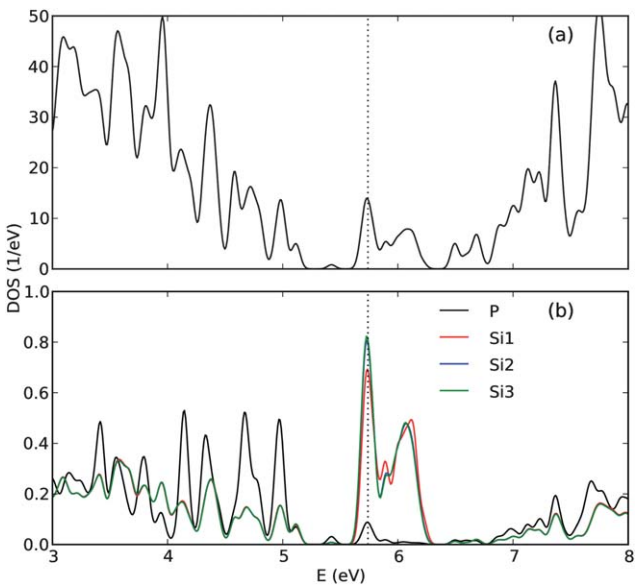

Fig. 4 (a) Total DOSs and (b) P 2s + 2p, Si 2s + 2p partial DOSs of atoms surrounding the vacancy in Si with P*V* defect.

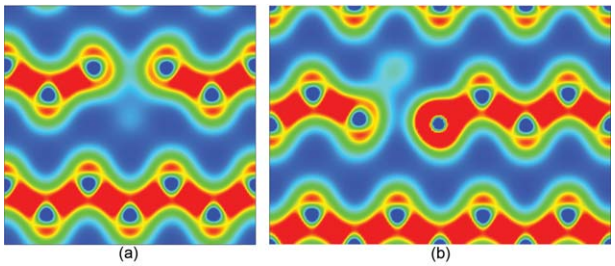

Fig. 5 Charge density of (a) the (101) plane and (b) the ($\bar{1}$01) plane in Si with P*V* defect. Blue and red colors correspond to low and high charge density, respectively.

around the *V* in Fig. 4. Integration of the total DOS from 5.3 eV to the Fermi energy yields exactly one electron, almost equally contributed by the three Si atoms, *i.e.*, the electron is not localized. Hence, the magnetic ordering in the P*V* cluster is weak and introduction of spin polarization hardly lowers the total energy. Since P gives only a very small contribution to the defect states, the two dangling electrons should be delocalized with low energy. The charge density maps depicted in Fig. 5 are consistent with the DOS analysis. The (101) plane shows Si chains and Si–Si bonds with high charge density. At the *V* the charge densities of the two adjacent Si atoms are still slightly connected. The distance between them amounts to 3.30 Å, which is much smaller than the distance between two next-nearest neighbor Si atoms in a perfect chain (3.84 Å). The charge density of the ($\bar{1}$01) plane shows the Si chains perpendicular to the (101) plane. Left and right of the *V*, respectively, we observe a Si and a P atom. This Si atom shows a connection of the charge to the two Si in the (101) plane.

Finally, it is anticipated that the formation of the PVO$_i$ defects will impact the diffusion of the VO$_i$ defects. In Si, the A-center diffuses faster than the E-center and it is expected that the formation of the very bound PVO$_i$ defects will retard the diffusion of the A-center. There is no study discussing the influence of P on VO$_i$ diffusion, however, previous studies established that the formation of highly bound clusters retard the A-center and E-center diffusion in Si and Ge.[24–28]

IV Summary

Electronic structure calculations have been employed to investigate the binding, ionization, and formation energies of PVO$_i$ defects in comparison to PV defects in Si. The difference in the stability between the two defects traces back to the interstitial O$_i$, which increases the binding energy significantly. The calculations reveal that PVO$_i^{+1}$ dominates up to a Fermi energy of 0.17 eV and PVO$_i^{-1}$ above 0.69 eV. The state in between turns out to be PVO$_i^{0}$ due to the spin polarization, whereas in a spin degenerate calculation this state would not appear. Analysis of the DOS demonstrates that the unoccupied defect state of PVO$_i^{+1}$ and fully occupied defect state of PVO$_i^{-1}$ are located between the valence and conduction bands, with which they merge in the case of PVO$_i^{0}$. The main part of the magnetic moment obtained for PVO$_i^{0}$ results from the dangling bond of the Si which is adjacent to the *V*. In addition, the dangling electron is found to be well delocalized in the PV^{0} cluster. Therefore, no spin polarization evolves in this case.

References

1 S. Takeuchi, Y. Shimura, O. Nakatsuka, S. Zaima, M. Ogawa and A. Sakai, *Appl. Phys. Lett.*, 2008, **92**, 231916.
2 A. Chroneos, C. A. Londos and E. N. Sgourou, *J. Appl. Phys.*, 2011, **110**, 093507.
3 E. Kamiyama, K. Sueoka and J. Vanhellemont, *J. Appl. Phys.*, 2012, **111**, 083507.
4 C. Gao, X. Ma, J. Zhao and D. Yang, *J. Appl. Phys.*, 2013, **113**, 093511.
5 W. Gao and A. Tkatchenko, *Phys. Rev. Lett.*, 2013, **111**, 045501.
6 R. C. Newman and R. Jones, Oxygen in silicon, in *Semiconductors and Semimetals*, ed. F. Shimura, Academic Press, Orlando, 1994, vol. 42, p. 289.
7 M. Cropper, A. Refregier, P. Guttridge, O. Boulade, J. Amiaux, D. Walton, P. Thomas, K. Rees, P. Pool, J. Endicott, A. Holland, J. Gow, N. Murray, A. Amara, D. Lumb, L. Duvet, R. Cole, J.-L. Augueres and G. Hopkinson, *Proc. SPIE*, 2010, **7731**, 77311J.
8 L. Lindegren, C. Babusiaux, C. Bailer-Jones, U. Bastian, A. G. A. Brown, M. Cropper, E. Høg, C. Jordi, D. Katz, F. van Leeuwen, X. Luri, F. Mignard, J. H. J. de Bruijne and T. Prusti, *Proc. Int. Astron. Union*, 2008, **248**, 217.
9 R. Massey, C. Stoughton, A. Leauthaud, J. Rhodes, A. Koekemoer, R. Ellis and E. Shaghoulian, *Mon. Not. R. Astron. Soc.*, 2010, **401**, 371.
10 A. Short, C. Crowley, J. H. J. de Bruijne and T. Prod'homme, *Mon. Not. R. Astron. Soc.*, 2013, **430**, 3078.
11 A. Chroneos, E. N. Sgourou and C. A. Londos, *J. Appl. Phys.*, 2012, **112**, 073706.
12 G. Kresse and D. Joubert, *Phys. Rev. B: Condens. Matter Mater. Phys.*, 1999, **59**, 1758.
13 P. E. Blöchl, *Phys. Rev. B: Condens. Matter Mater. Phys.*, 1994, **50**, 17953.
14 H. J. Monkhorst and J. D. Pack, *Phys. Rev. B: Solid State*, 1976, **13**, 5188.
15 J. P. Perdew, A. Ruzsinszky, G. I. Csonka, O. A. Vydrov, G. E. Scuseria, L. A. Constantin, X. Zhou and K. Burke, *Phys. Rev. Lett.*, 2008, **100**, 136406.
16 L. Schimka, J. Harl and G. Kresse, *J. Chem. Phys.*, 2011, **134**, 024116.
17 J. Heyd, G. E. Scuseria and M. Ernzerhof, *J. Chem. Phys.*, 2003, **118**, 8207.
18 J. P. Perdew, M. Ernzerhof and K. Burke, *J. Chem. Phys.*, 1996, **105**, 9982.
19 C. Freysoldt, J. Neugebauer and C. G. Van de Walle, *Phys. Rev. Lett.*, 2009, **102**, 016402.
20 C. Freysoldt, J. Neugebauer and C. G. Van de Walle, *Phys. Status Solidi B*, 2011, **248**, 1067.
21 J. Paier, M. Marsman and G. Kresse, *Phys. Rev. B: Condens. Matter Mater. Phys.*, 2008, **78**, 121201(R).

22 S. Lany and A. Zunger, *Phys. Rev. B: Condens. Matter Mater. Phys.*, 2008, **78**, 235104.
23 J. Heyd, J. E. Peralta, G. E. Scuseria and R. L. Martin, *J. Chem. Phys.*, 2005, **123**, 174101.
24 A. Chroneos, R. W. Grimes and H. Bracht, *J. Appl. Phys.*, 2009, **106**, 063707.
25 A. Chroneos, R. W. Grimes, B. P. Uberuaga and H. Bracht, *Phys. Rev. B: Condens. Matter Mater. Phys.*, 2008, **77**, 235208.
26 G. Impellizzeri, S. Boninelli, F. Priolo, E. Napolitani, C. Spinella, A. Chroneos and H. Bracht, *J. Appl. Phys.*, 2011, **109**, 113527.
27 A. Chroneos, C. A. Londos, E. N. Sgourou and P. Pochet, *Appl. Phys. Lett.*, 2011, **99**, 241901.
28 H. A. Tahini, A. Chroneos, R. W. Grimes, U. Schwingenschlögl and H. Bracht, *Phys. Chem. Chem. Phys.*, 2013, **15**, 367.